Control Engineering Practice 20 (2012) 674–683

Contents lists available at SciVerse ScienceDirect

Control Engineering Practice

journal homepage: www.elsevier.com/locate/conengprac

Laser pulse shaping via extremum seeking ☆

Beibei Ren [a,*], Paul Frihauf [a], Robert J. Rafac [b], Miroslav Krstic [a]

[a] Department of Mechanical and Aerospace Engineering, University of California, San Diego 9500 Gilman Drive, La Jolla, CA 92093-0411, USA
[b] Cymer Inc., 17075 Thornmint Court, San Diego, CA 92127, USA

ARTICLE INFO

Article history:
Received 13 July 2011
Accepted 11 March 2012
Available online 29 March 2012

Keywords:
Extremum seeking
Optimization
Laser
Pulse shaping

ABSTRACT

Extremum seeking, a non-model based optimization scheme, is employed to design laser pulse shapes that maximize the amount of stored energy extracted from the amplifier gain medium for a fixed input energy and inversion density. For this pulse shaping problem, a double-pass laser amplifier whose dynamics are fully coupled and composed of two nonlinear, first-order hyperbolic partial differential equations, with time delays in the boundary conditions, and a nonlinear ordinary differential equation, is considered. These complex dynamics make the optimization problem difficult, if not impossible, to solve analytically and make the application of non-model based optimization techniques necessary. Hence, the laser pulse shaping problem is formulated as a finite-time optimal control problem, which is solved by first, parameterizing the input pulse and pumping rate over the system's finite time interval and then, utilizing extremum seeking to maximize the associated cost function. The advantage of the approach is that the model information is not required for optimization. The extremum seeking methodology reveals that a rather non-obvious laser pumping rate waveform increases the laser gain by inducing a resonant response in the laser's nonlinear dynamics. Numerical simulations illustrate the effectiveness of the approach proposed in the paper.

1. Introduction

Background and motivation: Maximizing the energy extracted by a laser pulse is critical in many laser applications. In the polysilicon process for manufacturing flat panel displays, one of the outstanding problems is obtaining enough instantaneous laser power to melt as large an area as desired (e.g., one continuous melt of several meters along the substrate for a flat panel TV display). One engineering solution is to use several laser amplifiers and combine their outputs, but using a single amplifier more efficiently is preferable. The energy efficiency is also a growing concern in photolithography, where a drive to increase scanner wafer-per-hour throughout means that the optical exposures (which have a fixed energy dose required to print an image, set by the chemistry of the photoresist) must be accomplished with fewer pulses of higher energy. The goal in this paper is to optimize laser pulse shapes to maximize the amount of stored energy extracted from the amplifier gain medium for a fixed input energy and inversion density.

In Frantz and Nodvik (1963), the growth of a radiation pulse in a laser amplifier was described by nonlinear, time-dependent photon transport equations, which account for the effect of the radiation on the medium as well as vice versa. In Akashi, Sakai, and Tagashira (1995), a one-dimensional model including Poisson's equation to consider the space-charge for a discharge-excited ArF excimer laser has been developed. In the recent work (Ren, Frihauf, Krstić, & Rafac, 2011), a single-pass laser model is described by a coupled nonlinear first-order hyperbolic partial differential equation (PDE) and a nonlinear ordinary differential equation (ODE). This model is extended from the classical model (Frantz & Nodvik, 1963). In this paper, a double-pass laser model is considered with partial overlap and optical feedback in the amplifier, which adds another PDE and time delays in the boundary conditions. This setup allows for more efficient energy extraction and a longer output pulse length.

Design tool—extremum seeking: For two coupled first-order PDEs, with nonlinear coupling of Lotka–Volterra type, boundary control was developed in Pavel and Chang (2009) to drive the state at the end of the spatial domain to the desired constant reference values. Instead of stabilization, the laser pulse shape optimization problem is addressed in this paper. However, the complex dynamics in the laser amplifier model makes the optimization problem difficult, if not impossible, to solve analytically and make the application of non-model based optimization techniques necessary. The extremum seeking method (Ariyur & Krstić, 2003) is employed to design the finite-time optimal input signal and pumping rate to maximize the amount of stored

☆ This paper was not presented at any IFAC meeting.

* Corresponding author. Tel.: +1 858 822 1374; fax: +1 858 822 3107.
E-mail addresses: bren@ucsd.edu (B. Ren), pfrihauf@ucsd.edu (P. Frihauf), Robert_Rafac@cymer.com (R.J. Rafac), krstic@ucsd.edu (M. Krstic).

0967-0661/$ - see front matter © 2012 Elsevier Ltd. All rights reserved.
doi:10.1016/j.conengprac.2012.03.006

energy extracted from the amplifier gain medium for a fixed input energy and inversion density.

Extremum seeking is a real-time, non-model based optimization approach for dynamic problems where the system is assumed to have a potentially nonlinear equilibrium map with local minima or maxima, but is otherwise unknown. This method performs optimization by estimating the gradient of a cost function and driving this gradient to zero. The gradient estimation is performed using perturbation signals that are typically deterministic periodic signals, e.g., sinusoids (Ariyur & Krstić, 2003), but can be replaced by stochastic excitation signals (Liu & Krstić, 2010; Manzie & Krstić, 2009), or existing disturbances affecting the system (Carnevale et al., 2009). A popular tool in control applications in the 1940–1950s, extremum seeking has seen a resurgence after its stability analysis was established in Krstić and Wang (2000) for continuous-time systems and in Choi, Krstić, Ariyur, and Lee (2002) for discrete-time systems. Many successful applications of extremum seeking have been reported in the literature, including particle beam matching (Schuster et al., 2007), flow control (Becker, King, Petz, & Nitsche, 2007), tokamak fusion devices (Ou et al., 2008), source seeking with nonholonomic unicycles (Cochran, Kanso, Kelly, Xiong, & Krstić, 2009; Zhang, Arnold, Ghods, Siranosian, & Krstić, 2007), control of combustion instability (Banaszuk, Ariyur, Krstić, & Jacobson, 2004), maximizing the pressure rise in an axial flow compressor (Wang, Yeung, & Krstić, 2000), limit cycle minimization (Wang & Krstić, 2000), optimal positioning of mobile sensors under stochastic noise (Stanković & Stipanović, 2010), control of thermoacoustic instability (Moase, Manzie, & Brear, 2010), and optical fibre amplifiers (Dower, Farrell, & Nesić, 2008). However, extremum seeking has never before been used in high-performance photolithography light source systems.

Results: Motivated by Frihauf, Krstić, and Başar (2011), where extremum seeking was introduced to solve noncooperative games with infinitely-many players, the laser pulse shaping problem is formulated as a finite-time optimal control problem, by parameterizing the evolution of the input pulse and pumping rate in the time interval [0,T], and employing extremum seeking to maximize the associated cost function. Both a Gaussian input pulse shape parameterization and a general input pulse shape parameterization that consists of a summation of weighted finite characteristic functions are considered. The advantage of the approach is that modeling information of the laser amplifier is not required in the pulse shaping optimization via extremum seeking, and the effectiveness of this approach is shown through numerous simulations. Though the optimal pulse shape may not converge to the same shape for different initial conditions, the amplifier gain does improve for each case. In general, it is difficult to achieve global optimization using extremum seeking when multiple extrema exist (Tan, Nesic, Mareels, & Astolfi, 2009), which is expected for the high-dimensional extremum seeking problem considered in this paper. A rather non-obvious laser pumping rate waveform, which increases the laser gain by inducing a resonant response in the laser's nonlinear dynamics, is obtained using the extremum seeking approach.

Organization: The optimization problem is formulated in Section 2 and solved using extremum seeking for a Gaussian input peak timing optimization in Section 3 and a general input pulse shape optimization in Section 4. In Section 5, both the input pulse and the pumping rate are optimized simultaneously. Throughout this work, the effectiveness of the proposed method is demonstrated by extensive numerical studies. Finally, some concluding remarks are given in Section 6.

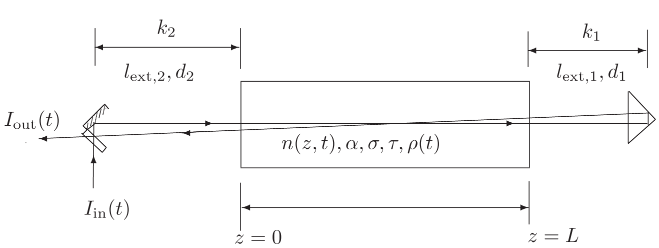

Fig. 1. Double-pass laser amplifier with partial overlap and optical feedback.

2. Double-pass laser dynamics with partial overlap and optical feedback

The intensity dynamics of the laser beam in Fig. 1 are described as follows for $z \in (0,L], t \geq 0$:

$$\begin{cases} \dfrac{\partial I_{\mathrm{lr}}(z,t)}{\partial t} &= -c\dfrac{\partial I_{\mathrm{lr}}(z,t)}{\partial z}+\sigma c n(z,t) I_{\mathrm{lr}}(x,t) \\ & \quad -\alpha I_{\mathrm{lr}}(z,t), \\ \dfrac{\partial I_{\mathrm{rl}}(z,t)}{\partial t} &= c\dfrac{\partial I_{\mathrm{rl}}(z,t)}{\partial z}+\sigma c n(z,t) I_{\mathrm{rl}}(z,t) \\ & \quad -\alpha I_{\mathrm{rl}}(z,t), \\ \dfrac{\partial n(z,t)}{\partial t} &= -\dfrac{1}{F_{\mathrm{sat}}}[I_{\mathrm{lr}}(z,t)+I_{\mathrm{rl}}(z,t)]n(z,t) \\ & \quad -\dfrac{1}{\tau}n(z,t)+\rho(t), \end{cases} \tag{1}$$

with boundary conditions

$$\begin{cases} I_{\mathrm{lr}}(0,t) &= k_2 I_{\mathrm{rl}}(0,t-2d_2)+(1-k_2)I_{\mathrm{in}}(t-d_2), \\ & \quad \text{boundary condition/input}, \\ I_{\mathrm{rl}}(L,t) &= k_1 I_{\mathrm{lr}}(L,t-2d_1), \\ & \quad \text{boundary condition}, \\ I_{\mathrm{out}}(t) &= (1-k_2)I_{\mathrm{rl}}(0,t-d_2)+k_2 I_{\mathrm{in}}(t), \\ & \quad \text{boundary value/output}, \end{cases} \tag{2}$$

where I_{lr} and I_{rl} are the rightward and leftward irradiance, respectively, n is the population difference between the upper and lower laser levels, and ρ is the pumping rate, k_1 and k_2 are partial overlap and optical feedback gains, $l_{\mathrm{ext},1}$ and $l_{\mathrm{ext},2}$ are the right and left extended lengths, and $d_1 = l_{\mathrm{ext},1}/c$ and $d_2 = l_{\mathrm{ext},2}/c$ are time delays caused by the extended lengths. The physical meanings and values of the parameters are listed in Table 1.

The objective is to seek the optimal input pulse shape $I_{\mathrm{in}}(t)$ over the time interval $t \in [0,T]$ such that the amplifier gain

$$\mathcal{G} = \frac{E_{\mathrm{out}}}{E_{\mathrm{in}}}, \tag{3}$$

Table 1
Parameters of the laser system.

Parameter	Description	Value (units)
L	Length of gain medium	0.5 (m)
T	Evolution duration time of laser dynamics	300 (ns)
c	Speed of light	3×10^8 (m/s)
σ	Stimulated emission cross section	2.8×10^{-16} (cm^2)
α	Distributed loss	0.006 (cm^{-1})
τ	Lifetime of laser state	1.75 (ns)
F_{sat}	Saturation fluence	3.67 ($\mathrm{mJ/cm}^2$)
k_1	Partial overlap gain	0.85
k_2	Optical feedback gain	0.95
$l_{\mathrm{ext},1}$	Extended length (right)	0.7 (m)
$l_{\mathrm{ext},2}$	Extended length (left)	0.8 (m)
d_1	Time delay (right)	2.3 (ns)
d_2	Time delay (left)	2.7 (ns)
E_{in}	Input energy	Fixed
E_{out}	Output energy	To be optimized
V_ρ	Inversion density	Fixed
$\mathcal{G} = \frac{E_{\mathrm{out}}}{E_{\mathrm{in}}}$	Amplifier gain	To be optimized

i.e., the ratio of the output energy $E_{\text{out}} = \int_0^T I_{\text{out}}(t)\,dt$ to the input energy $E_{\text{in}} = \int_0^T I_{\text{in}}(t)\,dt$, is maximized while holding the input energy and the inversion density $V_\rho = \int_0^T \rho(t)\,dt$ fixed. Hence, $I_{\text{in}}(t)$ needs to be found to solve

$$\max_{I_{\text{in}}(t) \geq 0} \mathcal{G} \quad \text{subject to } E_{\text{in}} \text{ and } V_\rho \text{ fixed.} \tag{4}$$

To ensure that the input energy and the inversion density are fixed, the input signal and the pumping rate are modulated over the period [0,T] as

$$I_{\text{in}}^{\text{mod}}(t) = \frac{I_{\text{in}}(t)}{\int_0^T I_{\text{in}}(t)\,dt} E_{\text{in}}^0, \tag{5}$$

$$\rho^{\text{mod}}(t) = \frac{\rho(t)}{\int_0^T \rho(t)\,dt} V_\rho^0, \tag{6}$$

where E_{in}^0 and V_ρ^0 are the user-defined input energy level and inversion density, respectively.

In the following subsections, the response of the double-pass laser models (1)–(2) is investigated with different input pulse shapes and pumping rates, highlighting their effect on the output pulse $I_{\text{out}}(t)$. Since the analytical solution of the models (1)–(2) is difficult, if not impossible, to find, the *implicit* finite difference approximation method (Tveito & Winther, 1998) is adopted to obtain its approximate solution. The space [0,L] is discretized into N_z intervals and the time interval [0,T] into N_t intervals with the spatial discretization $dz = L/N_z$ and temporal discretization $dt = T/N_t$. For the simulations, the parameters are chosen as N_z=100, N_t=1000, and thus dz=0.5 cm, dt=0.3 ns.

2.1. Response with Gaussian input pulse and pumping rate

Consider the case when both the input pulse and pumping rate are approximated by the Gaussian functions of time t

$$I_{\text{in}}(t) = \frac{1}{\sqrt{2\pi}\sigma_{\text{in}}} e^{-((t-\mu_{\text{in}})^2/2\sigma_{\text{in}}^2)}, \tag{7}$$

$$\rho(t) = A_\rho \frac{1}{\sqrt{2\pi}\sigma_\rho} e^{-((t-\mu_\rho)^2/2\sigma_\rho^2)}, \tag{8}$$

where μ_{in} and μ_ρ are the mean values (peak times), σ_{in} and σ_ρ are the standard deviations (pulse "width"), and A_ρ is the magnitude of pumping rate.

Fig. 2 shows the output pulse $I_{\text{out}}(t)$ with different Gaussian pumping rate magnitudes A_ρ, when μ_{in} and μ_ρ, σ_{in} and σ_ρ are fixed. It can be seen that $I_{\text{out}}(t)$ increases in magnitude and becomes more oscillatory when A_ρ increases. Fig. 3 shows the output pulse $I_{\text{out}}(t)$ with different pulse widths σ_ρ of the Gaussian pumping rate. With the increase of σ_ρ, the oscillations of $I_{\text{out}}(t)$ are reduced, but the magnitude of $I_{\text{out}}(t)$ decreases too. The amplifier gain $\mathcal{G}$ for Fig. 3(a), (b), and (c) is 139.32, 68.95 and 46.10, respectively, for the fixed inversion density $V_\rho^0 = 5 \times 10^{21}$ m^{-3}.

2.2. Response with constant input pulse and sinusoidal pumping rate

The modulation of the pumping rate are introduced in the following form:

$$\rho(t) = A_\rho[1 + \alpha_\rho \sin(2\pi\nu_\rho t)], \tag{9}$$

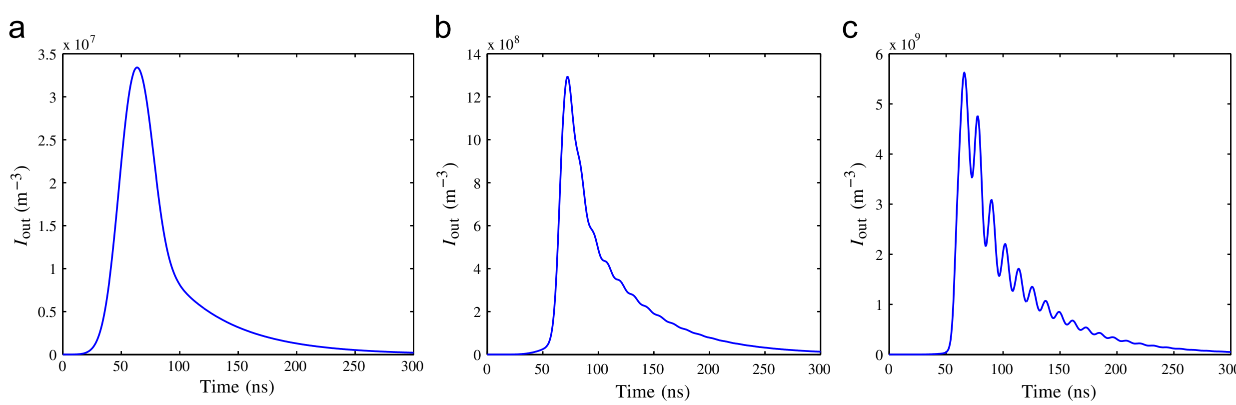

Fig. 2. Output pulse with different Gaussian pumping rate magnitudes A_ρ, while $\mu_{\text{in}} = \mu_\rho = 60$ ns, and $\sigma_{\text{in}} = \sigma_\rho = 12.8$ ns. (a) $A_\rho = 1 \times 10^{21}$ m^{-3} s^{-1}, (b) $A_\rho = 5 \times 10^{21}$ m^{-3} s^{-1}, and (c) $A_\rho = 10 \times 10^{21}$ m^{-3} s^{-1}.

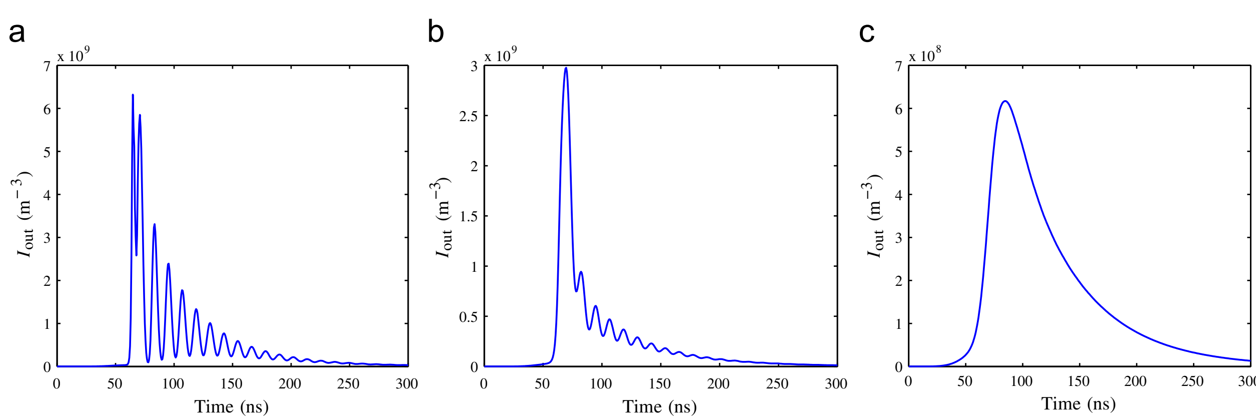

Fig. 3. Output pulse with different Gaussian pumping rate pulse widths σ_ρ, and while $A_\rho = 5 \times 10^{21}$ m^{-3} s^{-1}, $\mu_{\text{in}} = \mu_\rho = 60$ ns and $\sigma_{\text{in}} = 12.8$ ns. (a) $\sigma_\rho = 3$ ns, (b) $\sigma_\rho = 8$ ns, and (c) $\sigma_\rho = 20$ ns.

where υ_ρ is the modulation frequency, α_ρ is the modulation depth, and A_ρ is modulation mean. The effect of υ_ρ, α_ρ and A_ρ on the response of laser dynamics is investigated and illustrated in Figs. 4–6. In Fig. 4, the fixed inversion density is $V_\rho^0 = 5 \times 10^{22}$ m^{-3} over the period [0,T], while the amplifier gain is 51.76, 51.41, and 51.26 for (a), (b), and (c), respectively. In Fig. 5, the increase of A_ρ results in the increase of the inversion density, and thus, the increase of the amplifier gain. In particular, for Fig. 5 (a), (b), and (c), the inversion density is 7×10^{20} m^{-3}, 7×10^{21} m^{-3}, 7×10^{22} m^{-3}, and the corresponding amplifier gain is 1.18, 2.28 and 54.16, respectively. In Fig. 6, the fixed inversion density is $V_\rho^0 = 5 \times 10^{22}$ m^{-3} over the period [0,T], while the amplifier gain is 51.45, 51.48, and 51.04 for (a), (b), and (c), respectively.

From Figs. 2–6, it is noted that the performance of the double-pass laser model (1)–(2) is affected by the shapes of input pulse $I_{in}(t)$ and pumping rate $\rho(t)$. In the following sections, the pulse shaping optimization problem (4) is investigated for Gaussian peak timing optimization, where the input signal is Gaussian, and for a general input pulse shape, parameterized by the summation of weighted finite characteristic functions. Finally, both the input pulse shape and the pumping rate are optimized simultaneously.

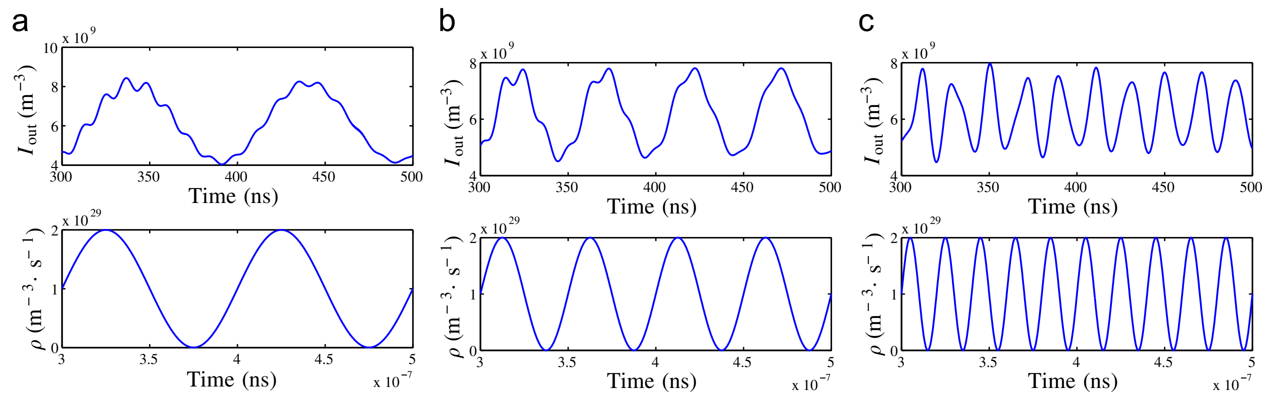

Fig. 4. Response with different sinusoidal pumping rate modulation frequencies υ_ρ, while $A_\rho = 1 \times 10^{29}$ m^{-3} s^{-1}, $\alpha_\rho = 1$, and $I_{in}(t) = 1 \times 10^8$ m^{-3}. (a) $\upsilon_\rho = 1 \times 10^7$, (b) $\upsilon_\rho = 2 \times 10^7$, and (c) $\upsilon_\rho = 5 \times 10^7$.

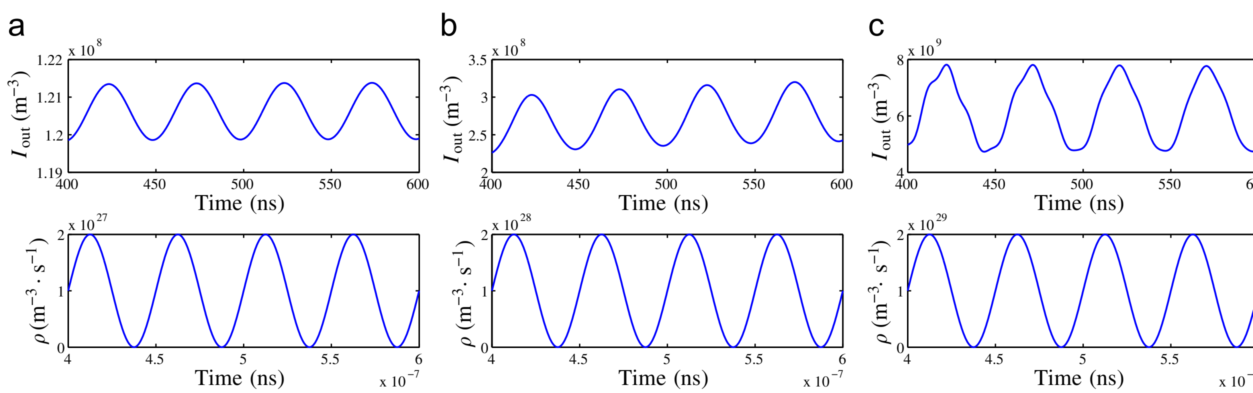

Fig. 5. Response with different sinusoidal pumping rate modulation mean magnitudes A_ρ, while $\upsilon_\rho = 2 \times 10^7$, $\alpha_\rho = 1$, and $I_{in}(t) = 1 \times 10^8$ m^{-3}. (a) $A_\rho = 1 \times 10^{27}$ m^{-3} s^{-1}, (b) $A_\rho = 1 \times 10^{28}$ m^{-3} s^{-1}, and (c) $A_\rho = 1 \times 10^{29}$ m^{-3} s^{-1}.

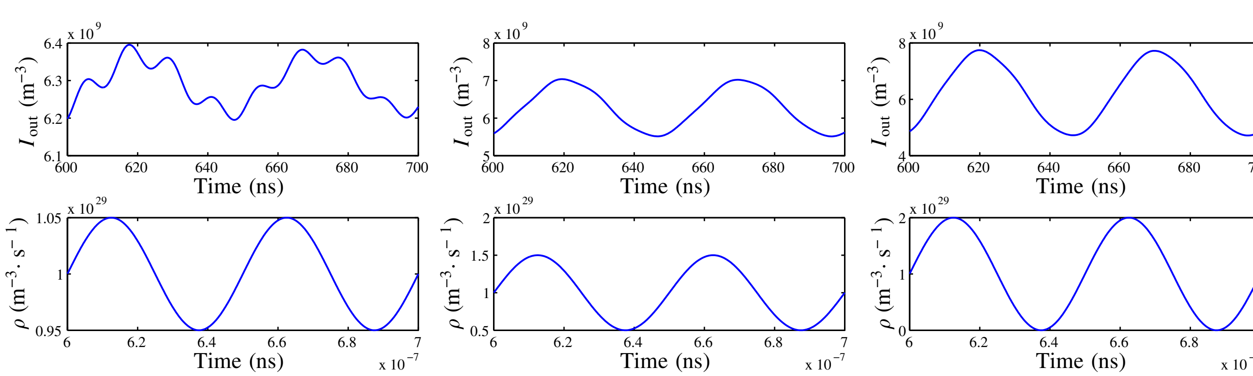

Fig. 6. Response with different sinusoidal pumping rate modulation depths α_ρ, while $A_\rho = 1 \times 10^{29}$ m^{-3} s^{-1}, $\upsilon_\rho = 2 \times 10^7$, and $I_{in}(t) = 1 \times 10^8$ m^{-3}. (a) $\alpha_\rho = 0.05$, (b) $\alpha_\rho = 0.5$, and (c) $\alpha_\rho = 1$.

3. Gaussian input peak timing optimization using extremum seeking scheme

Let both the input pulse and the pumping rate be modeled as Gaussian functions shown in (7) and (8). The objective is to find an optimal peak timing μ_{in} for the input pulse, so that the amplifier gain is maximized for a fixed input energy, with the pulse width σ_{in} and pumping rate $\rho(t)$ given. The optimization problem (4) is reformulated as

$$\max_{\mu_{\text{in}}>0} \quad \mathcal{G}$$

$$\text{subject to} \quad \sigma_{\text{in}}, \rho(t) \text{ given and } \int_0^T I_{\text{in}}(t)\,dt = E_{\text{in}}^0. \tag{10}$$

To solve the optimization problem (10), discrete-time extremum seeking is used to tune the parameter $\mu_{\text{in}}(k)$, where k is the discrete-time index, to determine the Gaussian-shaped input pulse $I_{\text{in}}(t)$ that optimizes the amplifier gain. Specifically, given a peak time $\mu_{\text{in}}(k)$, which determines the input pulse $I_{\text{in}}^k(t)$, the output pulse $I_{\text{in}}^k(t)$ is found and amplifier gain $\mathcal{G}^k$ is computed. The extremum seeking loop, driven by $\mathcal{G}^k$, updates the peak time parameter estimate to obtain $\mu_{\text{in}}(k+1)$ and the new input pulse $I_{\text{in}}^{k+1}(t)$. The process is then repeated.

A block diagram of the system is shown in Fig. 7, where $\hat{\mu}_{\text{in}}$ is the estimate of μ_{in}, γ^μ is the adaptation gain, ω_l and ω_h are low and high pass filter cutoff frequencies, $a \sin \omega k$ is the perturbation signal, and $\omega \in (0,\pi)$ is the perturbation frequency. In equation form, the extremum seeking algorithm is given by

$$\eta(k+1) = (1-\omega_h)\eta(k) + \omega_h \mathcal{G}^k, \tag{11}$$

$$\xi(k+1) = (1-\omega_l)\xi(k) + \omega_l(\mathcal{G}^k - \eta(k))a \sin \omega k, \tag{12}$$

$$\hat{\mu}_{\text{in}}(k+1) = \hat{\mu}_{\text{in}}(k) + \gamma^\mu \xi(k), \tag{13}$$

$$\mu_{\text{in}}(k) = \hat{\mu}_{\text{in}}(k) + a \sin \omega k. \tag{14}$$

The high pass filter removes the DC component of the cost function, and the low pass filter attenuates the oscillations caused by the sinusoidal perturbation and smooths the parameter estimate $\hat{\mu}_{\text{in}}$. The stability of the extremum seeking feedback scheme can be established by employing the tools of averaging and singular perturbation analysis (Ariyur & Krstić, 2003; Choi et al., 2002; Krstić & Wang, 2000).

Simulation results: In this study, the initial $I_{\text{in}}(t)$ and $\rho(t)$ are taken as the form of (7) and (8) with $A_{\text{in}} = 1.0\ \text{m}^{-3}$, $\mu_{\text{in}} = 60$ ns, $\sigma_{\text{in}} = 12.8$ ns, while $A_\rho = 4 \times 10^{21}\ \text{m}^{-3}\ \text{s}^{-1}$, $\mu_\rho = 60$ ns, $\sigma_\rho = 3$ ns. The initial amplifier gain $\mathcal{G}^0 = 86.76$. Other extremum seeking parameters in Fig. 7 are chosen as: $\gamma^\mu = 1$, $a = 0.6$, $\omega = 1$, $\omega_l = 0.024$, $\omega_h = 0.020$. Fig. 8 shows the evolution of the amplifier gain $\mathcal{G}$ and Gaussian input peak timing μ_{in} when μ_{in} is tuned using extremum seeking. It can be seen that the optimal amplifier gain $\mathcal{G}^* = 93.76$ and optimal peak time $\mu_{\text{in}}^* = 44.97$ ns are achieved after 1000 extremum seeking steps. Thus, when the amplifier gain $\mathcal{G}$ is maximized, the Gaussian peak time of the input signal is 15.03 ns ahead of the pumping rate peak.

4. General input pulse shaping optimization

In Section 3, using extremum seeking, the peak time for the scaled Gaussian single-hump function has been optimized to maximize the amplifier gain. However, the amplifier gain may potentially be increased further by more complex input pulse shapes that cannot be modeled by Gaussian single-humps. Therefore, in this section the general input pulse shaping optimization problem is considered.

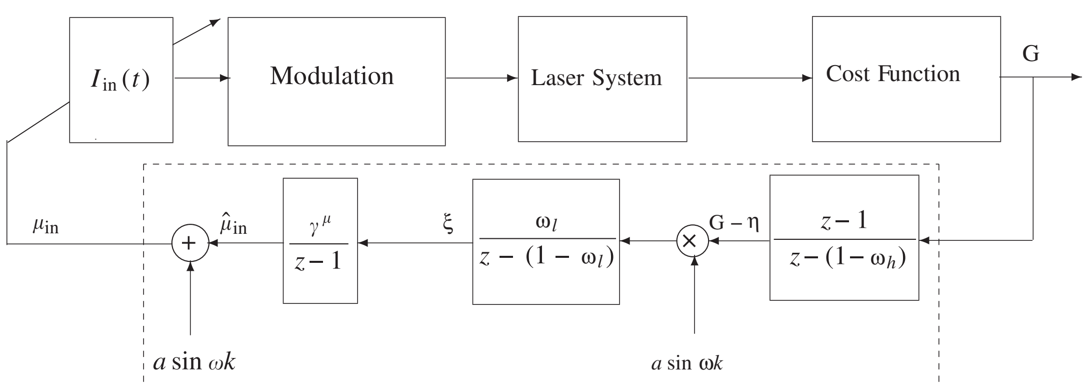

Fig. 7. Discrete-time extremum seeking scheme for Gaussian input peak timing optimization.

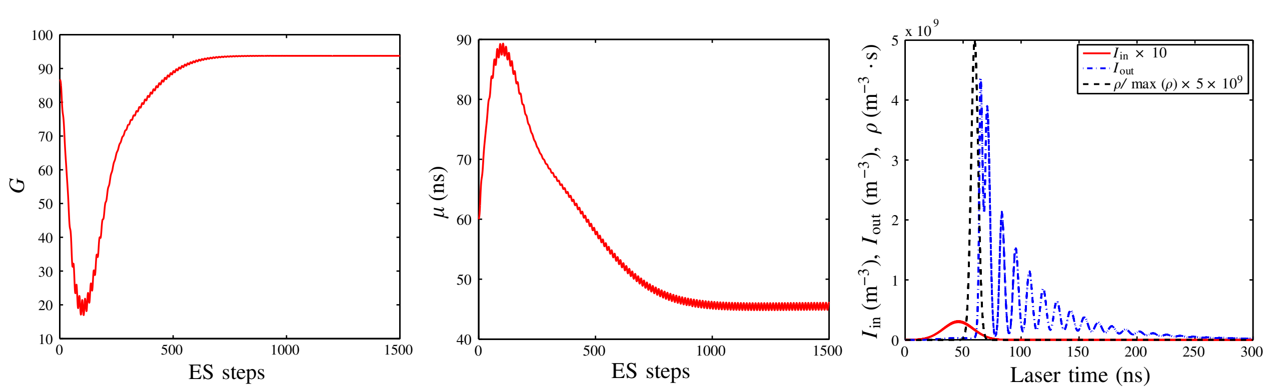

Fig. 8. The evolution of the amplifier gain $\mathcal{G}$ (a) and Gaussian input peak time μ_{in} (b) using extremum seeking when $\sigma_{\text{in}} = 12.8$ ns; and (c) the pumping rate ρ, optimal input I_{in}, and output signal I_{out}.

Motivated by Frihauf et al. (2011), where extremum seeking was introduced to solve noncooperative games with infinitely-many players, the problem in this paper is formulated as an infinite-dimensional optimal control problem by the parametrization of the evolution of the input pulse $I_{in}(t)$ in the time interval $[0,T]$. The input pulse $I_{in}(t)$, $t\in[0,T]$ is approximated in the space $L^2[0,T]$ as follows:

$$I_{in}(t)=\sum_{j=1}^{N}\theta_j\mathbf{1}_{[t_j,t_{j+1}]}(t),\quad t\in[t_j,t_{j+1}],\tag{15}$$

where $[0,T]$ is divided into a finite number (N) of intervals $[t_j,t_{j+1}]$, $j=1,2,\ldots,N$, with $t_1=0$, $t_{N+1}=T$, θ_j is the weight for the jth characteristic function, and $\mathbf{1}_{[t_j,t_{j+1})}(t)$ denotes the characteristic function in the interval $[t_j,t_{j+1}]$, i.e.

$$\mathbf{1}_{[t_j,t_{j+1}]}(t)=\begin{cases}1, & t\in[t_j,t_{j+1}),\\ 0 & \text{otherwise}.\end{cases}\tag{16}$$

Extremum seeking is applied to determine optimal values for the weights θ_j.

In practice, some constraints on the input function $I_{in}(t)$ have to be considered due to the dynamics and magnitude constraints in the electronics that generate the input signal. For example, $I_{in}(t)$ cannot be too short or too long in duration, and $I_{in}(t)$ cannot change too rapidly. The constraints on the input pulse shape can be adjusted by σ_{in} when a Gaussian-like shape is assumed as is done in Section 3. For a general input pulse, however, there is no direct control over the optimized shape; therefore, a penalty on the input gradient is included in the cost function to penalize overly narrow input signals, resulting in the following optimization problem:

$$\max_{\theta>0}\quad J(\theta)\ \text{with}\ J(\theta)=\mathcal{G}-\beta\int_0^T(\dot{I}_{in})^2(t)\,dt$$
$$\text{subject to}\quad \rho(t)\ \text{given and}\ \int_0^T I_{in}(t)\,dt=E_{in}^0,\tag{17}$$

where $\beta>0$ is the penalty weight, $\theta=[\theta_1,\theta_2,\ldots,\theta_N]^T$ is defined in (15), and E_{in}^0 is a user-defined input energy level. In simulation (or in practice, when sampling the continuous-time laser amplifier dynamics (1)–(2)), the idealized, integral penalty term in (17) must be approximated. In this work, a forward finite-difference approximation is adopted for the time derivative of the input pulse, namely

$$\begin{aligned}\dot{I}_{in}(t_j)&\approx\frac{I_{in}(t_{j+1})-I_{in}(t_j)}{dt},\quad j=1,2,\ldots,N_t,\\ &=\frac{\theta_{j+1}-\theta_j}{dt},\end{aligned}\tag{18}$$

where $dt=T/N$. The integral term is then approximated by a Riemann sum, i.e.

$$\begin{aligned}\int_0^T(\dot{I}_{in})^2(t)\,dt&\approx\sum_{j=1}^{N}\left(\frac{\theta_{j+1}-\theta_j}{dt}\right)^2dt,\\ &=\frac{1}{dt}\sum_{j=1}^{N}(\theta_{j+1}-\theta_j)^2.\end{aligned}\tag{19}$$

The multi-parameter extremum seeking scheme used to maximize (17) is

$$\eta(k+1)=(1-\omega_h)\eta(k)+\omega_hJ(\theta(k)),\tag{20}$$

$$\xi_j(k+1)=(1-\omega_l)\xi_j(k)+\omega_l(J(\theta(k))-\eta(k))a_j\sin\omega_jk,\tag{21}$$

$$\hat{\theta}_j(k+1)=\hat{\theta}_j(k)+\gamma_j^\theta\xi(k),\tag{22}$$

$$\theta_j(k)=\hat{\theta}_j(k)+a_j\sin\omega_jk,\tag{23}$$

where, for $j=1,2,\ldots,N$, $\hat{\theta}_j$ is the estimate of the optimal weight vector θ^*, γ_j^θ is the adaptation gain, ω_l and ω_h are low and high pass filter cutoff frequencies, $a_j\sin\omega_jk$ is the perturbation signal, and $\omega_j\in(0,\pi)$ is the perturbation frequency. For multi-parameter extremum seeking designs, the perturbation frequencies must also satisfy $\omega_i\neq\omega_j$, $i\neq j$ (Durr, Stanković, & Johansson, 2011). The extremum seeking scheme used to update θ_j is depicted in Fig. 9.

Simulation results: The simulation results are shown in Figs. 10–12, where the time interval $[0,T]$ for the laser amplifier dynamics has been discretized into $N=500$ intervals. In Fig. 10, the initial and final signal pulse shapes for the input $I_{in}(t)$ and the output $I_{out}(t)$ are shown in (a) and (b), and the evolution of the cost $J(\theta)$ and amplifier gain $\mathcal{G}$ are depicted in (c). The initial input pulse is chosen as a single-hump shape with energy $E_{in}^0=1.0\ \text{m}^{-3}$ s, and penalty weight $\beta=2.25\times10^{-25}\ \text{m}^6$ s (where the penalty weight β units are given so that the cost $J(\theta)$ is a nondimensional value). The pumping rate $\rho(t)$ is described by a Gaussian function as (8) with $A_\rho=4\times10^{21}\ \text{m}^{-3}\ \text{s}^{-1}$, $\mu_\rho=60$ ns, $\sigma_\rho=3$ ns.

The extremum seeking parameters are selected as $a=[a_1,a_2,\ldots,a_N]^T$, $\omega=[\omega_1,\omega_2,\ldots,\omega_N]^T$ and γ^θ by a random draw from a uniform distribution. Specifically, a is sampled from the distribution $U^a(2\times10^6,4\times10^6)$, ω from $U^\omega(0.3,0.6)$, and $\gamma^\theta=[\gamma_1^\theta,\gamma_2^\theta,\ldots,\gamma_N^\theta]^T$ from $U^\gamma(0.3,0.4)$, where $U(a,b)$ denotes the uniform distribution with probability density $1/(b-a)$. Note, the probability that $\omega_i=\omega_j$ is zero. One could also choose ω as the value of a monotonically increasing or decreasing function so that $\omega_i\neq\omega_j$. ω is selected from a uniform distribution so that comparatively fast and slow frequencies are spread throughout the parameter space. The low pass and high pass filter parameters are $\omega_l=0.024$ and $\omega_h=0.020$.

It is observed that:

(i) The optimal cost $J^*=130.82$ and optimal amplifier gain $\mathcal{G}^*=134.54$ are achieved after 1.0×10^5 extremum seeking

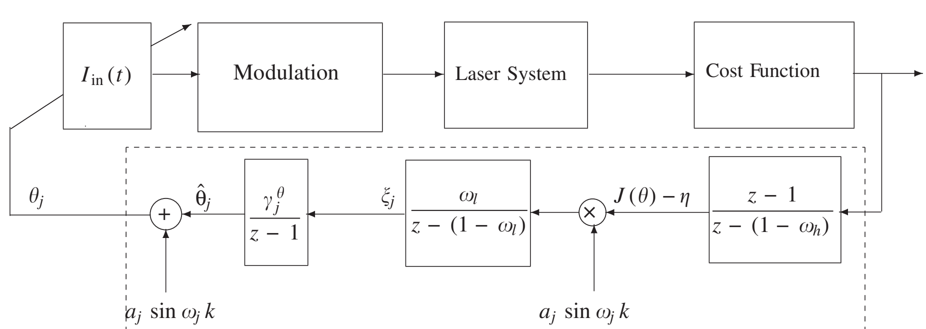

Fig. 9. Discrete-time extremum seeking scheme for general input pulse shaping with the θ_j loop depicted.

steps, while the initial cost $J^0 = 93.70$ and initial amplifier gain $\mathcal{G}^0 = 93.71$.
(ii) The input pulse shape converges to an optimal multi-hump pulse.

While Fig. 10 shows a result with a single-hump initial pulse, Fig. 11 shows a result with a double-hump initial input signal pulse. Similar results are obtained though the initial input pulse is different. In Fig. 12 the effect of the penalty weight β on the performance is investigated, where $\beta = 6.75 \times 10^{-24}$ m^6 s and the initial input pulse is double-hump. Based on Figs. 11 and 12, it is observed that:

(i) The peak value of the optimal input pulse decreases and the duration of the pulse increases, i.e., its rate of change decreases as β is increased.
(ii) The achieved amplifier gain and extremum seeking convergence rate both decrease as β is increased.

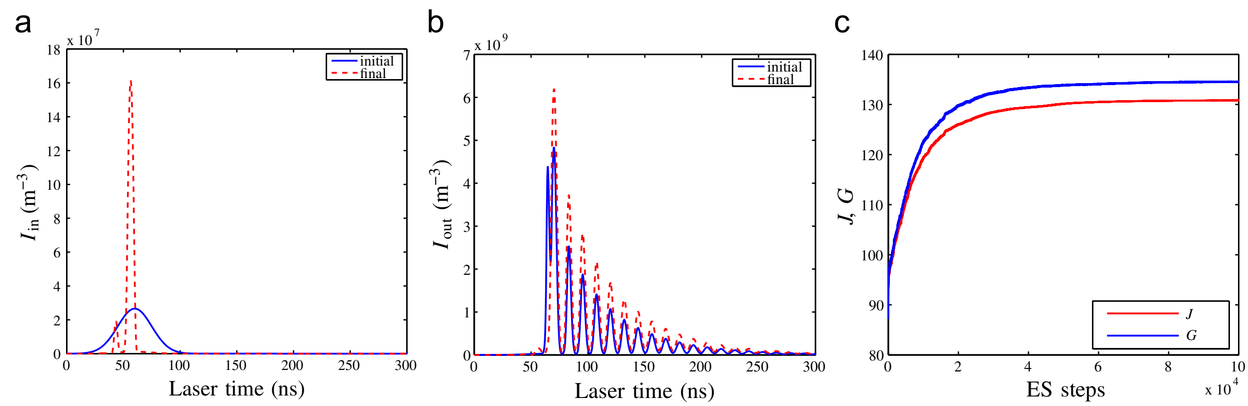

Fig. 10. Initial and final (a) input $I_{in}(t)$ and (b) output $I_{out}(t)$ signals when using the extremum seeking algorithm with $N=500$ for a single-hump initial input pulse, and (c) the evolution of the cost function $J(\theta)$ and amplifier gain $\mathcal{G}$. Convergence is achieved in 4.0×10^4 steps, when $A_\rho = 4 \times 10^{21}$ m^{-3} s^{-1}, $\mu_\rho = 60$ ns, $\sigma_\rho = 3$ ns, and $E^0_{in} = 1.0$ m^{-3} s and the penalty weight $\beta = 2.25 \times 10^{-25}$ m^6 s.

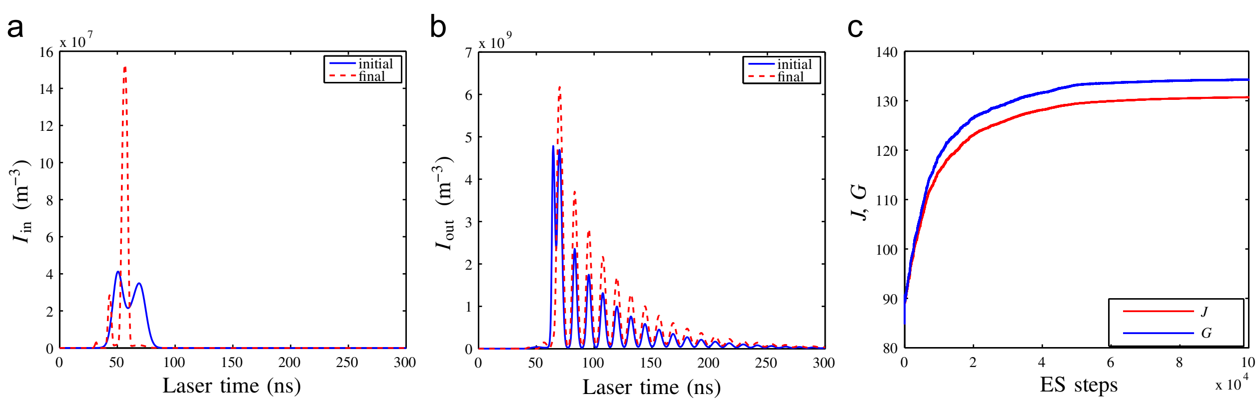

Fig. 11. Initial and final (a) input $I_{in}(t)$ and (b) output $I_{out}(t)$ signals when using the extremum seeking algorithm with $N=500$ for a double-hump initial input pulse, and (c) the evolution of the cost function $J(\theta)$ and amplifier gain $\mathcal{G}$. Convergence is achieved in 4.0×10^4 steps, when $A_\rho = 4 \times 10^{21}$ m^{-3} s^{-1}, $\mu_\rho = 60$ ns, $\sigma_\rho = 3$ ns, and $E^0_{in} = 1.0$ m^{-3} s and the penalty weight $\beta = 2.25 \times 10^{-25}$ m^6 s.

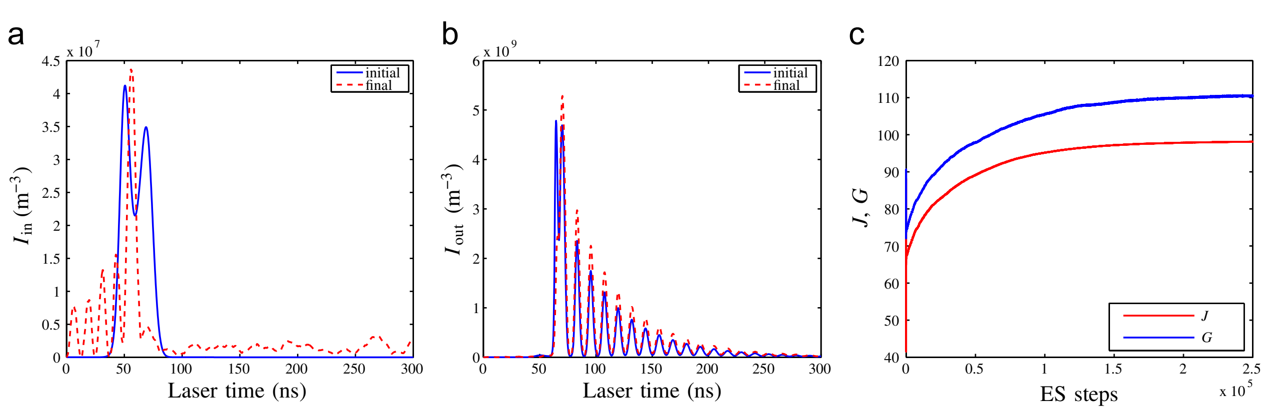

Fig. 12. Results with the same conditions as in Fig. 11 except for the penalty weight $\beta = 6.75 \times 10^{-24}$ m^6 s. Convergence is achieved in 2.0×10^5 steps, when $A_\rho = 4 \times 10^{21}$ m^{-3} s^{-1}, $\mu_\rho = 60$ ns, $\sigma_\rho = 3$ ns, and $E^0_{in} = 1.0$ m^{-3} s and the penalty weight $\beta = 2.25 \times 10^{-24}$ m^6 s.

(iii) It is not surprising that the extremum seeking scheme could converge to one of the local extrema if they exist, in particular, for the high-dimensional extremum seeking problem considered in this paper. For different initial conditions and cost function parameters, the optimal pulse shape may not converge to the same shape, however, the amplifier gain does improve indeed for each case.

5. Optimization of both input pulse and pumping rate

In Sections 3 and 4, the input pulse $I_{in}(t)$ has been optimized with the pumping rate $\rho(t)$ given. Now extremum seeking is used to optimize both $I_{in}(t)$ and $\rho(t)$ to maximize the extraction of the stored energy from the amplifier gain medium.

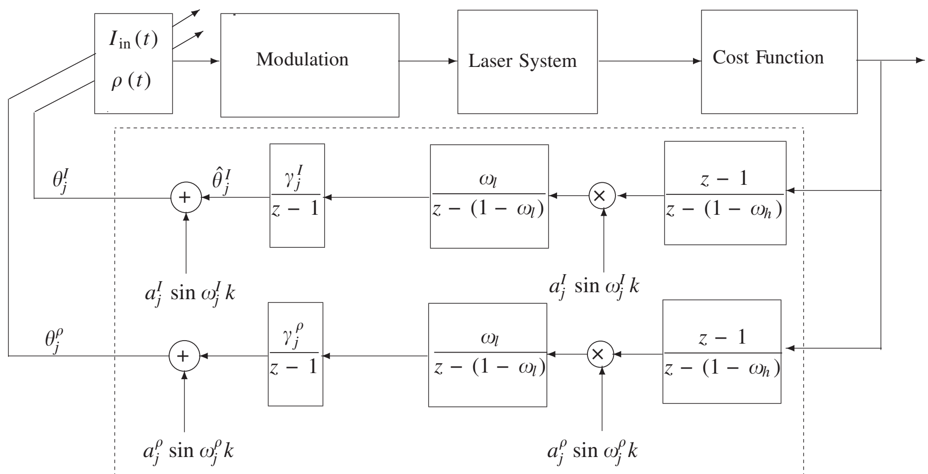

Fig. 13. Discrete-time extremum seeking scheme for both input pulse shaping and pumping rate pulse shaping optimization with loops for θ_j^I and θ_j^ρ shown.

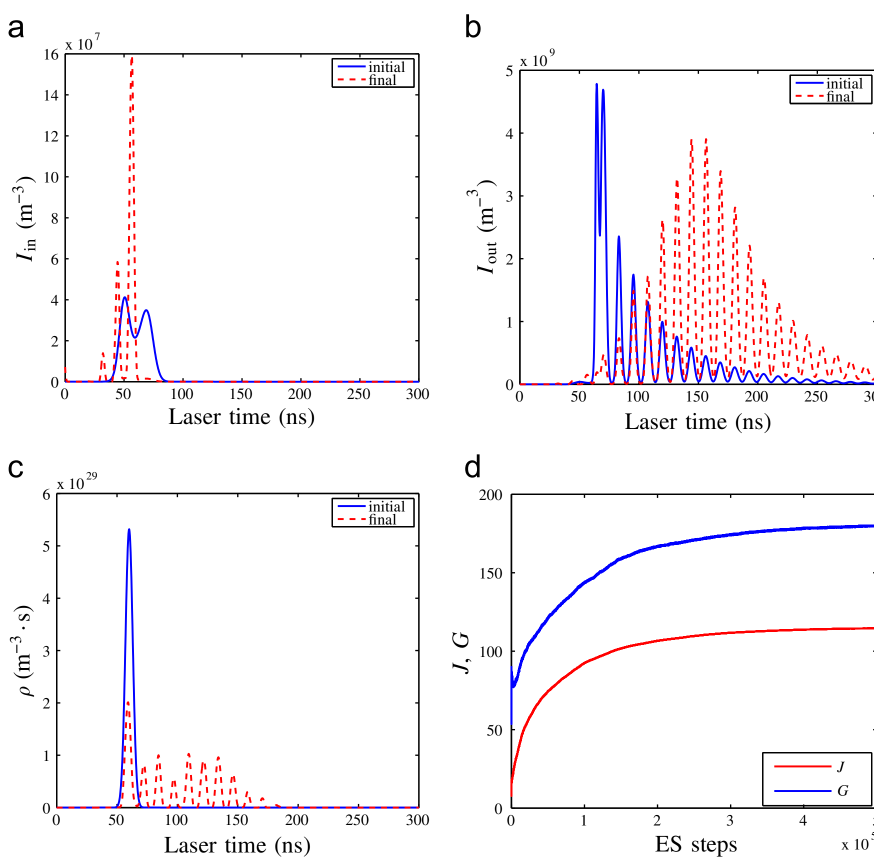

Fig. 14. Initial and final (a) input $I_{in}(t)$, (b) output $I_{out}(t)$ and (c) pumping rate $\rho(t)$ signals when using the extremum seeking algorithm with $N=500$ for a double-hump initial input pulse, and (d) the evolution of the cost function $J(\theta)$ and amplifier gain $\mathcal{G}$. Convergence is achieved in 5.0×10^4 steps, when $E_{in}^0 = 1.0$ m^{-3} s, $V_\rho^0 = 4.0 \times 10^{21}$ m^{-3} and the penalty weights $\beta = 2.25 \times 10^{-25}$ m^6 s, $\gamma = 9 \times 10^{-67}$ m^6 s^3.

It is assumed that the input pulse $I_{\text{in}}(t)$ and pumping rate $\rho(t)$, $t \in [0,T]$, are approximated in the space $L^2[0,T]$ as follows:

$$I_{\text{in}}(t) = \sum_{j=1}^{N} \theta_j^I \mathbf{1}_{[t_j,t_{j+1}]}(t), \quad t \in [t_j,t_{j+1}] \tag{24}$$

$$\rho(t) = \sum_{j=1}^{N} \theta_j^\rho \mathbf{1}_{[t_j,t_{j+1}]}(t), \quad t \in [t_j,t_{j+1}] \tag{25}$$

where $[0,T]$ is separated into N intervals $[t_j,t_{j+1}]$, $j=1,2,\ldots,N$, $t_1=0$ and $t_{N+1}=T$, and where $\mathbf{1}_{[t_j,t_{j+1}]}(t)$ denotes the characteristic function given by (16). The weights for the jth characteristic function of $I_{\text{in}}(t)$ and $\rho(t)$ are denoted by θ_j^I and θ_j^ρ, respectively.

Due to practical constraints on the input function $I_{\text{in}}(t)$ and the pumping rate $\rho(t)$, both a penalty on the input gradient and a penalty on the pumping rate gradient are included in the cost function to prevent $I_{\text{in}}(t)$ and $\rho(t)$ from having a rapid rate of change. Hence, the optimization problem becomes

$$\max_{\theta^I>0,\theta^\rho>0} \quad J(\theta^I,\theta^\rho),$$

$$\text{with} \quad J(\theta^I,\theta^\rho) = \mathcal{G} - \beta \int_0^T (\dot{I}_{\text{in}})^2(t)\,dt - \gamma \int_0^T (\dot{\rho})^2(t)\,dt$$

$$\text{subject to} \quad \int_0^T I_{\text{in}}(t)\,dt = E_{\text{in}}^0, \; \int_0^T \rho(t)\,dt = V_\rho^0, \tag{26}$$

where $\beta > 0$ and $\gamma > 0$ are the penalty weights for the input gradient and the pumping rate gradient, $\theta^I = [\theta_1^I,\theta_2^I,\ldots,\theta_N^I]^T$ and $\theta^\rho = [\theta_1^\rho,\theta_2^\rho,\ldots,\theta_N^\rho]^T$, which are defined in (24) and (25), and $V_\rho^0 = \int_0^T \rho^0(t)\,dt$. In implementation, the integral penalty terms are numerically approximated as is done in Section 4 (cf. (17)–(19)).

The multi-parameter extremum seeking scheme used to maximize (26) are

$$\eta(k+1) = (1-\omega_h)\eta(k) + \omega_h J(\theta^I(k),\theta^\rho(k)), \tag{27}$$

$$\xi_j^I(k+1) = (1-\omega_l)\xi_j^I(k) + \omega_l (J(\theta^I(k),\theta^\rho(k)) - \eta(k)) a_j^I \sin \omega_j^I k, \tag{28}$$

$$\hat{\theta}_j^I(k+1) = \hat{\theta}_j^I(k) + \gamma_j^I \xi^I(k), \tag{29}$$

$$\theta_j^I(k) = \hat{\theta}_j^I(k) + a_j^I \sin \omega_j^I k, \tag{30}$$

$$\xi_j^\rho(k+1) = (1-\omega_l)\xi_j^\rho(k) + \omega_l (J(\theta^I(k),\theta^\rho(k)) - \eta(k)) a_j^\rho \sin \omega_j^\rho k, \tag{31}$$

$$\hat{\theta}_j^\rho(k+1) = \hat{\theta}_j^\rho(k) + \gamma_j^\rho \xi^\rho(k), \tag{32}$$

$$\theta_j^\rho(k) = \hat{\theta}_j^\rho(k) + a_j^\rho \sin \omega_j^\rho k, \tag{33}$$

where $j=1,2,\ldots,N$, $\theta^I(k)$ and $\theta^\rho(k)$ are the weight vectors of $I_{\text{in}}(t)$ and $\rho(t)$ to be optimized; $\hat{\theta}^I(k)$ and $\hat{\theta}^\rho(k)$ are the estimates of $\theta^I(k)$ and $\theta^\rho(k)$, respectively; and $a^I \sin \omega^I k$, and $a^\rho \sin \omega^\rho k$ are perturbation signals. The extremum seeking scheme is depicted in Fig. 13.

Simulation results: Fig. 14(a)–(c) show the initial and final signal pulse shapes for the input $I_{\text{in}}(t)$, output $I_{\text{out}}(t)$, and pumping rate $\rho(t)$ signals, respectively, when the time interval $[0,T]$ is discretized into $N=500$ intervals. The evolution of the cost $J(\theta^I,\theta^\rho)$ and amplifier gain $\mathcal{G}$ is also shown in Fig. 14(d). The extremum seeking parameters ω_l, ω_h, and those used to tune θ^I are the same as those selected in simulations presented in Section 4. And $a^\rho = [a_1^\rho,a_2^\rho,\ldots,a_N^\rho]$ is sampled from the distribution $U_\rho^a(2\times10^{27},4\times10^{28})$, ω^ρ from $U_\rho^\omega(0.3,0.6)$, and $\gamma^\rho = [\gamma_1^\rho,\gamma_2^\rho,\ldots,\gamma_N^\rho]^T$ from $U_\rho^\gamma(0.1,0.2)$, where $U(a,b)$ denotes the uniform distribution with probability density $1/(b-a)$.

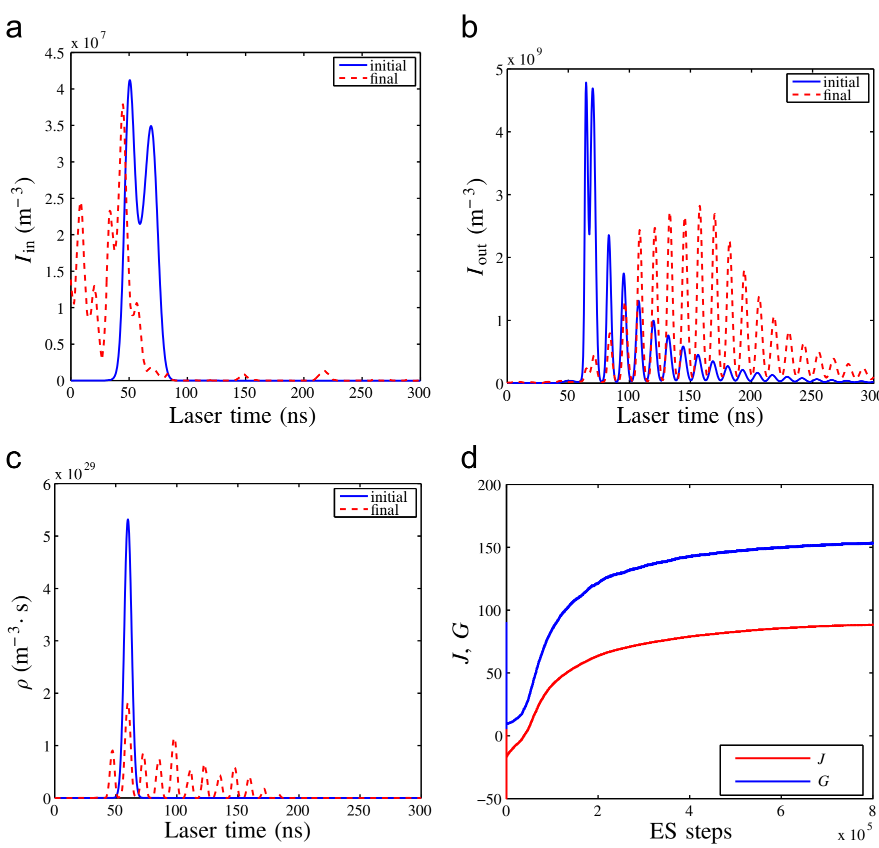

Fig. 15. Initial and final (a) input $I_{\text{in}}(t)$, (b) output $I_{\text{out}}(t)$ and (c) pumping rate $\rho(t)$ signals when using the extremum seeking algorithm with $N=500$ for a double-hump initial input pulse, and (d) the evolution of the cost function $J(\theta)$ and amplifier gain $\mathcal{G}$. Convergence is achieved in 5.0×10^4 steps, when $E_{\text{in}}^0 = 1.0$ m^{-3} s, $V_\rho^0 = 4.0\times10^{21}$ m^{-3} and the penalty weights $\beta = 6.75\times10^{-24}$ m^6 s, $\gamma = 9\times10^{-67}$ m^6 s^3.

For the fixed input energy $E_{\text{in}} = 1.0\ \text{m}^{-3}$ s, inversion density $V_\rho = 4.0 \times 10^{21}\ \text{m}^{-3}$ and penalty weights $\beta = 2.25 \times 10^{-25}\ \text{m}^6$ s, $\gamma = 9.0 \times 10^{-67}\ \text{m}^6\ \text{s}^3$:

(i) the optimal cost $J^* = 114.59$ and optimal amplifier gain $\mathcal{G}^* = 179.83$ are achieved after 5×10^5 extremum seeking steps, while the initial cost $J^0 = 15.22$ and initial amplifier gain $\mathcal{G}^0 = 90.50$,
(ii) the input pulse converges from a double-hump pulse to an optimal three-hump pulse,
(iii) the pumping rate pulse also converges to an optimal multi-hump pulse, which seems to oscillate at a frequency that promotes a resonance in the laser dynamics, and
(iv) compared with the extremum seeking results in Fig. 11 when the pumping rate $\rho(t)$ is a given value, the energy amplifier gain is increased from 126.09 to 179.83.

Fig. 15 shows the effect of the penalty weight β on the performance where $\beta = 6.75 \times 10^{-24}\ \text{m}^6$ s. Compared with the results in Fig. 14, it can be seen that:

(i) The peak value of the optimal input pulse decreases and the duration of the pulse increases, i.e., its rate of change decreases when β is increased.
(ii) Both the achieved amplifier gain and extremum seeking convergence rate decrease when β is increased.
(iii) For different cost function parameters, the optimal pulse shape may not converge to the same shape. However, the amplifier gain does improve for each case.

A comparison of Figs. 12 and 15 (or Figs. 11 and 14) provides an interesting physical insight. Extremum seeking finds a non-obvious pumping rate $\rho(t)$ that improves the gain $\mathcal{G}$ by about 40% by inducing a resonant response in the laser dynamics.

6. Conclusion

In this paper the input pulse and pumping rate shape optimization have been investigated for a laser amplifier through the high-dimensional extremum seeking method. It has been shown that the optimized input/pumping rate signal can extract maximum stored energy from the amplifier gain medium for different initial conditions and different cost function parameters. No model information is required in the pulse shaping optimization. A non-obvious pumping rate $\rho(t)$ has been found to improve the gain $\mathcal{G}$ by about 40% by inducing a resonant response in the laser dynamics.

References

Akashi, H., Sakai, Y., & Tagashira, H. (1995). Modelling of a self-sustained discharge-excited ArF excimer laser: the influence of photo-ionization and photodetachment by laser light on the discharge development. *Journal of Physics D: Applied Physics*, *28*, 445–451.

Ariyur, K., & Krstić, M. (2003). *Real-time optimization by extremum seeking control*. Hoboken, NJ: Wiley-Interscience.

Banaszuk, A., Ariyur, K. B., Krstić, M., & Jacobson, C. A. (2004). An adaptive algorithm for control of combustion instability. *Automatica*, *40*(11), 1965–1972.

Becker, R., King, R., Petz, R., & Nitsche, W. (2007). Adaptive closed-loop separation control on a high-lift configuration using extremum seeking. *AIAA Journal*, *45*(6), 1382–1392.

Carnevale, D., Astolfi, A., Centioli, C., Podda, S., Vitale, V., & Zaccarian, L. (2009). A new extremum seeking technique and its application to maximize rf heating on ftu. *Fusion Engineering and Design*, *84*(2–6), 554–558.

Choi, J.-Y., Krstić, M., Ariyur, K. B., & Lee, J. S. (2002). Extremum seeking control for discrete-time systems. *IEEE Transactions on Automatic Control*, *47*(2), 318–323.

Cochran, J., Kanso, E., Kelly, S. D., Xiong, H., & Krstić, M. (2009). Source seeking for two nonholonomic models of fish locomotion. *IEEE Transactions on Robotics and Automation*, *25*(5), 1166–1176.

Dower, P. M., Farrell, P. M., & Nesić, D. (2008). Extremum seeking control of cascaded raman optical amplifiers. *IEEE Transactions on Control Systems Technology*, *16*(3), 396–407.

Durr, H.-B., Stanković, M. S., & Johansson, K. H. (2011). Distributed positioning of autonomous mobile sensors with application to coverage control. In *2011 American control conference*.

Frantz, L. M., & Nodvik, J. S. (1963). Theory of pulse propagation in a laser amplifier. *Journal of Applied Physics*, *34*(8), 2346–2349.

Frihauf, P., Krstić, M., & Başar, T. (2011). Nash equilibrium seeking with infinitely many players. In *2011 American control conference*.

Krstić, M., & Wang, H. H. (2000). Stability of extremum seeking feedback for general nonlinear dynamic systems. *Automatica*, *36*(4), 595–601.

Liu, S.-J., & Krstić, M. (2010). Stochastic averaging in continuous time and its applications to extremum seeking. *IEEE Transactions on Automatic Control*, *55*(10), 2235–2250.

Manzie, C., & Krstić, M. (2009). Extremum seeking with stochastic perturbations. *IEEE Transactions on Automatic Control*, *54*(3), 580–585.

Moase, W. H., Manzie, C., & Brear, M. J. (2010). Newton-like extremum-seeking for the control of thermoacoustic instability. *IEEE Transactions on Automatic Control*, *55*(9), 2094–2105.

Ou, Y., Xu, C., Schuster, E., Luce, T. C., Ferron, J., Walker, M. L., & Humphreys, D. A. (2008). Design and simulation of extremum-seeking open-loop optimal control of current profile in the DIII-D Tokamak. *Plasma Physics and Controlled Fusion*, *50*(3), 115001.

Pavel, L., & Chang, L. (2009). Lyapunov-based boundary control for 2×2 hyperbolic Lotka-Volterra systems. In *Joint 48th IEEE conference on decision and control and 28th Chinese control conference*.

Ren, B., Frihauf, P., Krstić, M., & Rafac, R. J. (2011). Laser pulse shaping via iterative learning control and infinite-dimensional extremum seeking. In *2011 ASME dynamic systems and control conference*.

Schuster, E., Xu, C., Torres, N., Morinaga, E., Allen, C., & Krstić, M. (2007). Beam matching adaptive control via extremum seeking. *Nuclear Instruments and Methods in Physics Research Section A: Accelerators, Spectrometers, Detectors and Associated Equipment*, *581*(3), 799–815.

Stanković, M. S., & Stipanović, D. M. (2010). Extremum seeking under stochastic noise and applications to mobile sensors. *Automatica*, *46*(8), 1243–1251.

Tan, Y., Nesic, D., Mareels, I. M. Y., & Astolfi, A. (2009). On global extremum seeking in the presence of local extrema. *Automatica*, *45*(1), 245–251.

Tveito, A., & Winther, R. (1998). *Introduction to partial differential a computational approach*. New York: Springer-Verlag.

Wang, H.-H., & Krstić, M. (2000). Extremum seeking for limit cycle minimization. *IEEE Transactions on Robotics and Automation*, *45*(12), 2432–2437.

Wang, H.-H., Yeung, S., & Krstić, M. (2000). Experimental application of extremum seeking on an axial-flow compressor. *IEEE Transactions on Control Systems Technology*, *8*(2), 300–309.

Zhang, C., Arnold, D., Ghods, N., Siranosian, A., & Krstić, M. (2007). Source seeking with nonholonomic unicycle without position measurement and with tuning of forward velocity. *Systems & Control Letters*, *56*(3), 245–252.